Hindawi
Journal of Electrical and Computer Engineering
Volume 2023, Article ID 5563242, 19 pages
https://doi.org/10.1155/2023/5563242

Research Article

Optimized Model Torque Prediction Control Strategy for BLDCM Torque Error and Speed Error Reduction System

Ye Yuan, Cheng Liu, Siyu Chen, and Zhenxiong Zhou

College of Electrical and Information Engineering, Beihua University, Jilin, China

Correspondence should be addressed to Cheng Liu; liucheng@beihua.edu.cn

Received 20 July 2023; Revised 7 August 2023; Accepted 8 August 2023; Published 25 August 2023

Academic Editor: R. Palanisamy

This paper presents an improved whale optimization algorithm (IWOA) for optimizing the model predictive torque control (MPTC) of brushless DC motor (BLDCM) to further reduce the problems of strong torque pulsation and high ripple caused by the special structure of BLDCM. IWOA adds a randomized convergence factor strategy to the original algorithm, enabling the parameter weights to be adjusted in time. The relative error between the training set and the predicted values is reduced, and a suitable interval is selected for the target. The proposed method takes into account the switching frequency loss factor in the MPTC system of BLDCM, discarding the traditional trial-and-error method and choosing to control the parameter adjustment by the degree of deviation. The IWOA is compared with the popular whale optimization algorithm (WOA), dragonfly algorithm (DA), ant colony optimization (ACO) algorithm, and grey wolf optimization (GWO) algorithm on the MATLAB SIMULINK platform to verify the effectiveness of the method in dealing with improved chain tracking, reduced torque pulsation, and reduced speed error. The simulation results show that IWOA performs well, with an efficiency of 94.32%.

1. Introduction

The BLDC motor body's stator winding is typically divided into multiple phases (three-phase, four-phase, and five-phase varies). The rotor consists of permanent magnets in a certain number of pole pairs [1–4]. When a phase of the stator winding is energized, the magnetic field generated by the current interacts with the magnetic field generated by the poles to drive the rotor, and then the position sensor converts the rotor position into an electrical signal to control the inverter so that each phase of the stator winding is energized in a certain order and the stator phase current changes phases in a certain order with the rotor position [5, 6].

It is very meaningful to reduce speed error and torque pulsation in brushless DC motors. Due to the influence of factors such as nonideal counterpotential waveform, tooth groove structure, and current commutation, leading to more obvious torque pulsation in BLDCM, which makes the motor operation noise and vibration increase and reduce the motor load carrying capacity and cannot be applied in the field of high-performance servo control, it is crucial to improve the torque dynamic response control performance of BLDCM for the popularization of the use of this motor; similarly, in the conventional speed control system of BLDCM, the conventional controller will make the speed overshoot too much, which will lead to the oscillation problem. Therefore, eliminating the speed overshoot problem of the speed controller plays a very crucial role in realizing the fast response of the motor speed and the minimization of the steady-state error, both of which are of great significance for the prospect of a simple and easy engineering application of BLDCM.

The continuous improvement of the research content of BLDC motors has prompted the reinvestigation of electric vehicles in BLDC motors. BLDC motors have a good response to the static and dynamic responses of the industry, prompting them to have a long-term impact on industry production, such as electric crank windows in cars, inverter washing machines, inverter air conditioners, small motors in optical drives, and many other BLDC devices [7–10].

However, BLDC motors can produce large torque fluctuations due to their own cogging structure, phase change currents, nonideal counterelectromotive force waveforms, and other factors. The presence of torque pulsation has limited the application of BLDC in servo systems, especially in direct drive applications where torque pulsation deteriorates the motor speed control characteristics, thus, suppressing or eliminating torque pulsation has become the key to improving the performance of servo systems [11, 12].

A common issue with direct torque strategy in motors is large torque fluctuations at low speeds. Many advanced controllers have been proposed to solve this problem, with model torque prediction control (MPTC) strategies being the most prominent and incorporating advanced algorithms that are emerging into our vision. MPTC is generally used to accurately track the magnetic chain by weighing the chain and using torque weights to reduce torque ripple [13–16]. However, in practical conditions, the overreliance on empirical methods for the target weights does not provide much certainty about the actual errors that occur [17]. Also, the majority of MPTC is used in permanent magnet synchronous motor (PMSM), with little research done in BLDC motors.

The whale optimization algorithm was proposed by Mirjalili and Lewis in 2016, and they mentioned in the literature [18] that the algorithm was developed based on the unique bubble net foraging behavior of humpback whales. It has a strong search ability for multiobjective problems in terms of errors and can deal well with target-weighting interests. This is why it was chosen as the base algorithm for the optimization of MPTC systems in this paper.

The intention of this paper is to propose an IWOA to improve the MPTC of BLDC motor. The method adjusts the weighting parameter coefficients in a timely manner and analyzes the average switching frequency losses of the inverter to minimize torque ripple and accurately track flux performance.

This article has the following three main contributions: (a) IWOA is a modification of the WOA, incorporating the idea of simulated perturbations and using a random adjustment of the convergence factor strategy to reduce the relative error between the predicted and actual values. The proposed method is compared and analyzed on the MATLAB platform with advanced algorithms from recent years. (b) The traditional trial-and-error method of weighting in MPTC has been replaced by the advanced IWOA, which can quickly and accurately find the right interval for the target weights. The proposed method also takes into account the switching frequency losses of BLDC motor. (c) Considering the special structure of the BLDCM, the results are analyzed using speed and torque in two different cases, and the proposed method is able to cope with the different situations, combining the target weights to give a suitable output.

The remainder of the paper is organized as follows: Section 2 summarizes research reports from recent years, and in Section 3 the mathematical model of BLDCM is analyzed and the DTC and MPTC strategies are elaborated. In Section 4, the WOA is briefly described, and measures to improve the WOA are discussed in detail. The application of the algorithm to the MPTC of the BLDCM is presented in Section 5. Simulation results are given in Section 6 and are discussed and investigated in relation to the simulation results. Finally, the conclusions are presented.

2. A Brief Summary of Recent Research Reports

In terms of advanced control strategies, a diagonal recurrent neural network (QRNN) strategy based on the Q-learning algorithm was proposed in the literature [19], and the Q-learning algorithm was improved to optimize the weight momentum factor, which was accurately verified at different operating conditions and speeds of the BLDCM. Kommula et al. in the literature [20] show that with the help of a fractional order PID based on an improved firefly algorithm and a particle swarm algorithm controller based on a modified firefly algorithm and a particle swarm algorithm, the uncertainty due to load variations is reduced and the torque fluctuations are greatly reduced. Not coincidentally, in the literature [21], a fuzzy parametric adaptive PI controller was proposed using reference speed and feedback speed as input and deviation, and the steady-state error, overshoot, was analyzed under different speed reference responses to demonstrate the strong robustness brought by the method. The literature [22] uses the idea of neural networks on this basis, and in the results, better control can be achieved. In the literature [23], the Coyote algorithm is designed for controller parameter rectification, and control precision is improved through low-speed operation experiments. In the literature [24], generalized predictive fractional order PI control was combined with lion swarm optimization to enable the optimal signal to come into the system, and an experimental platform was built to verify the feasibility. A new copper loss minimizing DTC was proposed in the literature [25] to achieve BLDCM in DTC while achieving high efficiency and high torque fine reading, using a three-phase conduction voltage vector meter to achieve tracking control of the magnetic chain, cutting out the torque pulsation caused by the back EMF and nonideal phase change in the conventional two-phase conduction voltage vector meter DTC, and improving control accuracy. Cao et al. [26] produced a reflection on the BLDCM braking case and proposed a smooth torque control strategy for the BLDCM that corresponds to the direct torque control performance in different speed ranges according to different modulation methods to achieve controllability of the braking torque and also reduce the phase change torque. The literature [27] uses numerical analysis ideas in the optimization of MPTC systems to linearize the torque function and current constraints, eliminating gain tuning according to the characteristics of the control strategy. Choi et al. focuses attention on the complex weighting factors in MPTC, and proposes an online adjustment of the weighting factors in the literature [28] to keep the error within a certain range. Guazzelli et al. [29] propose the nondominant sorting genetic algorithm (NSGA-II), which lists torque, chain performance, and average switching frequency as the three target values from which the best value is selected. These

algorithms have some differences, with different convergence and accuracy, in that they all improve on the traditional DTC, but it is an important challenge to accurately track the magnetic chain and improve torque ripple using MPTC on a BLDCM, a motor with a special structure. In the literature [30], WOA is applied for the first time to optimize a hyperparameter problem, comparing it with a neural network algorithm and a random search method, two traditional algorithms that demonstrate the high accuracy of WOA. In the literature [31], the WOA algorithm was combined with adaptive convergence and Levi's characteristics to solve the problem of easily falling into local optima, reflecting good global search capabilities. Got et al. combined the WOA with a multiobjective problem in the literature [32], introducing the population profile whale optimization algorithm (GPAWOA), combining GPAWOA with the multiobjective particle swarm optimization (MOPSO) algorithm, decomposing the multiobjective evolutionary algorithm (MOEA/D), and using the multiobjective grey wolf optimization (MOGWO) algorithm for comparing results analysis. GPAWOA achieved good performance in convergence and population diversity and literature [33] proposed to combine WOA with a hybrid grey wolf optimization algorithm to eliminate the optimization error in the observer and the uncertainty of external disturbances in mechanical systems. In dealing with the inability to generate maximum power in BLDCM-based battery-free PV systems, the literature [34] combines WOA with conventional perturbation observation (P&O). In the literature [35], Nadimi-Shahraki et al. focus their attention on the problem of improving the WOA search capability by introducing two different motion strategies to enhance the WOA capability and validated by simulation.

3. BLDCM Mathematical Model and Traditional Control Strategy

3.1. BLDCM Mathematical Model. BLDCM is so named because it eliminates the need for a mechanical phase commutator and brushes and relies on an inverter to convert the DC current into a square wave motor. Figure 1 shows what a three-phase full-bridge inverter with a BLDCM looks like in terms of its circuit.

Here, $T_1 \sim T_6$ are six switches, where u_A, u_B, and u_C are the stator three-phase winding voltages; e_A, e_B, and e_C are the three-phase winding induced electromotive forces; and i_A, i_B, i_C are the stator currents in phases A, B, and C, respectively. U_d is the DC bus voltage, and C_d is the capacitance at DC. The voltage balance equation for the three-phase stator winding can be written as follows:

$$\begin{bmatrix} u_A \\ u_B \\ u_c \end{bmatrix} = \begin{bmatrix} R_s & 0 & 0 \\ 0 & R_s & 0 \\ 0 & 0 & R_s \end{bmatrix} \begin{bmatrix} i_A \\ i_B \\ i_C \end{bmatrix} + \begin{bmatrix} L_s - M & 0 & 0 \\ 0 & L_s - M & 0 \\ 0 & 0 & L_s - M \end{bmatrix} p \begin{bmatrix} i_A \\ i_B \\ i_c \end{bmatrix} + \begin{bmatrix} e_A \\ e_B \\ e_C \end{bmatrix}, \tag{1}$$

where R_s is the stator winding, L_s is the self-inductance of each phase winding, M is the phase-to-phase mutual inductance, and p is the differential operator.

Due to the inherent characteristics of brushless DC motors, the control frequently takes the form of a two-by-two conduction, as opposed to the sine wave magnetic field of three-phase asynchronous motors and permanent magnet synchronous motors. On the same bridge arm, the next two switching elements are 1 for on and 0 for off. Therefore, the six nonzero voltage vectors are represented in turn as u_1 (100001), u_2 (001001), u_3 (011000), u_4 (010010), u_5 (000110), and u_6 (100100). Figure 2(a) represents the switching tube state corresponding to each nonzero voltage vector in space, and Figure 2(b) represents each nonzero voltage vector in space schematically.

3.2. Conventional DTC for BLDCM. In a conventional DTC, a magnetic chain observer is required to calculate the stator magnetic chain, whereas the conventional method basically takes the stator terminal voltage and phase current as well as the stator resistance to calculate it. However, at low-speed operation, the stator voltage decreases, the stator side resistance is measured incorrectly, and the calculation has to go through the operation of integration, which can lead to distortion of the magnetic chain observation. Therefore, the magnetic chain estimation link is only used to estimate the current stator magnetic chain position; (2) and (3) are the u-i model equations, where the amplitude and amplitude angle of the stator magnetic chain are obtained from (4) and (5), respectively.

$$\psi_{s\alpha} = \int \left[u_{s\alpha} - R_s i_{s\alpha}\right] dt, \tag{2}$$

$$\psi_{s\beta} = \int \left[u_{s\beta} - R_s i_{s\beta}\right] dt, \tag{3}$$

$$\psi_s = \sqrt{\psi_{s\alpha}^2 + \psi_{s\beta}^2}, \tag{4}$$

$$\theta_e = \arcsin \frac{\psi_{s\beta}}{\psi_s}, \tag{5}$$

where $\psi_{s\alpha}$, $\psi_{s\beta}$, $i_{s\alpha}$, $i_{s\beta}$, $u_{s\alpha}$, and $u_{s\beta}$ are the stator magnetic chain, stator current components, and stator voltage in the α-β stationary coordinate system, respectively. R_s is the stator winding resistance.

Since the flux density of the BLDCM is distributed in a trapezoidal wave, the torque calculation in the DTC of asynchronous and permanent magnet synchronous motors are no longer used. Because the BLDCM stator resistance is very small and the effect of higher harmonics in the magnetic

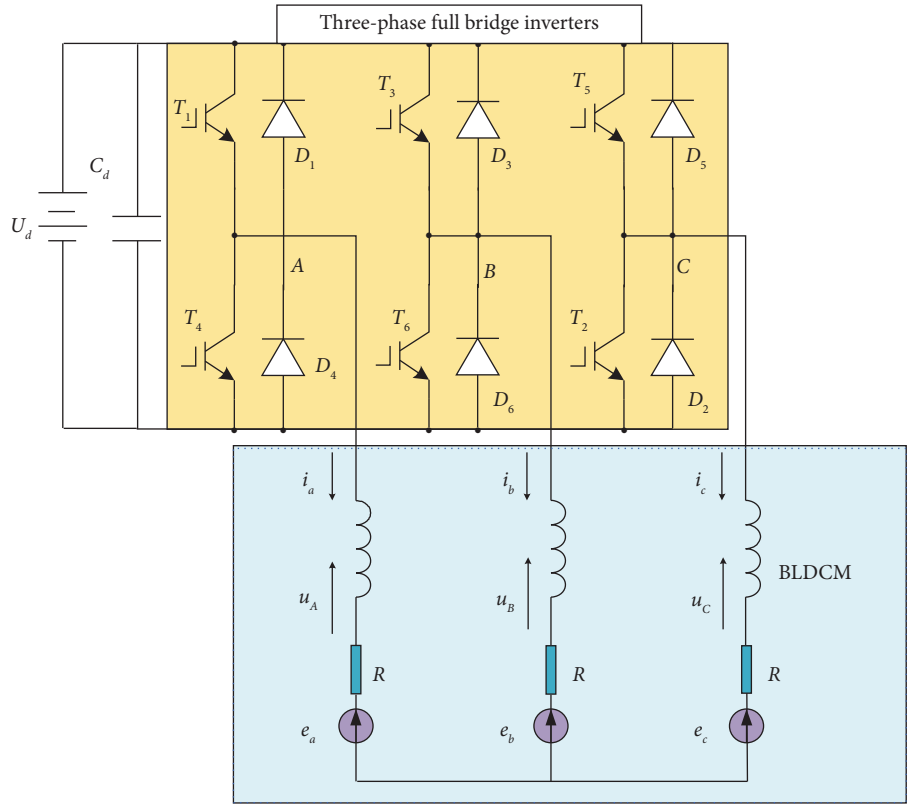

Figure 1: Equivalent circuit diagram of a three-phase full-bridge inverter with BLDCM.

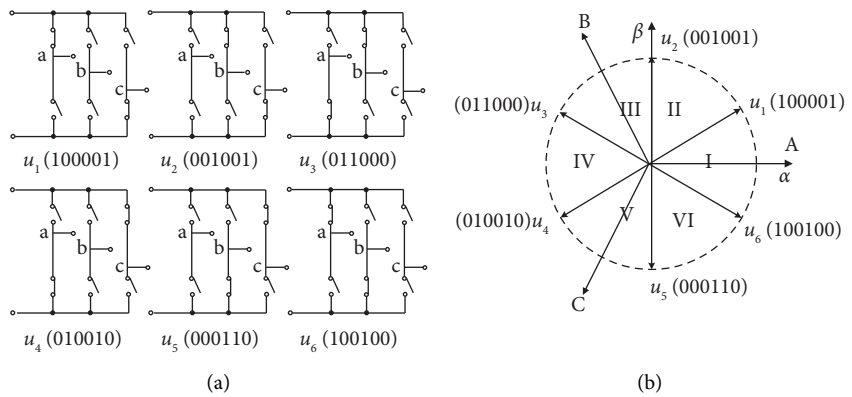

Figure 2: Conduction mode. (a) Switching tube state corresponding to nonzero spatial voltage vector. (b) Nonzero voltage vector in space diagram.

chain on the torque can be ignored, the electromagnetic torque is rewritten as given in the following equation. The space can be divided into six sectors according to the value of θ_e.

$$T_e = \frac{3}{2} p\left[\left(\frac{\mathrm{d}\varphi_{rd}}{\mathrm{d}\theta_e} - \varphi_{rq}\right) i_{sd} + \left(\frac{\mathrm{d}\varphi_{rq}}{\mathrm{d}\theta_e} + \varphi_{rd}\right) i_{sq}\right], \tag{6}$$

where θ_e is the rotor position angle, $\varphi_{rd}\varphi_{rq}i_{sd}i_{sq}$ are the stator magnetic chain, the component of the stator current on the two-phase rotating coordinate system (d-q), and p is the number of pole pairs of the motor.

To produce constant electromagnetic torque, a square wave stator current input is required, or when the stator current is square wave, the counterelectromotive force waveform is required to be a trapezoidal waveform. The duration of the square wave current is 120° electrical angles per half cycle, and either the flat top part of the trapezoidal counterelectromotive force is also 120° electrical angles, and the two should be strictly synchronized. At any given moment, only two phases of the stator are on.

The voltage equation for the three-phase winding of the BLDCM stator can be written in the form of an equation of state, as shown in the following equation:

$$p\begin{bmatrix} i_A \\ i_B \\ i_c \end{bmatrix} = \begin{bmatrix} \frac{1}{(L_s - M)} & 0 & 0 \\ 0 & \frac{1}{(L_s - M)} & 0 \\ 0 & 0 & \frac{1}{(L_s - M)} \end{bmatrix} \left(\begin{bmatrix} u_A \\ u_B \\ u_c \end{bmatrix} - \begin{bmatrix} R_s & 0 & 0 \\ 0 & R_s & 0 \\ 0 & 0 & R_s \end{bmatrix} \begin{bmatrix} i_A \\ i_B \\ i_c \end{bmatrix} - \begin{bmatrix} e_A \\ e_B \\ e_c \end{bmatrix} \right). \tag{7}$$

The basic idea of DTC is to divide the magnetic chain rotation space into 6 stages, set the tolerance of the magnetic chain and torque hysteresis loop according to the torque control requirements, compare the observed value of the torque with the given value, combine the stages of the stator magnetic chain, select the appropriate voltage vector, control the inverter directly, and output the corresponding space voltage vector to control the output torque of the motor. Figure 3 shows the basic schematic of the DTC.

3.3. BLDCM Conventional MPTC. MPTC is often based on the stator current, electromagnetic torque as the controlled object, and online rolling to solve for the optimal output quantity, which often requires a value function to evaluate the motor's operating state during this period. Rolling optimization is an important core part of MPTC, where the predicted model state at the kth moment in a control cycle is used to predict the output state for $k+1$. The state quantity is compared with the reference quantity output trajectory, and the value function is used to determine the optimal voltage vector. The above MPTC is not performed offline; it is an online prediction of the control quantities of the system. However, there are external disturbances, and the predicted value and the actual desired value often have unavoidable deviations. MPTC can usually be divided into finite-set predictive torque control (FCS-MPTC) and continuous-set predictive torque control (CCS-MPTC); this paper adopts FCS-MPTC. FCS-MPTC is easier to implement by substituting the voltage vector into the value function in turn and selecting the best quality by the value function's minimization constraint, but the degree of freedom of regulation is underground, which will lead to unstable switching frequency and overreliance on the motor's fixed parameters, making accurate control difficult. How to solve the switching frequency instability in the control strategy, where the system is overly dependent on parameters, is the focus of this thesis research.

In conventional FCS-MPTC, the prediction of the next cycle electromagnetic torque $T_e(k+1)$ and stator magnetic chain $\psi_s(k+1)$ is essential. The mathematical model of the stator magnetic chain is shown in the following equation, as the stator current prediction model is shown in (9) and the electromagnetic torque prediction model is shown in (10).

$$\psi_{s,dq}(k+1) = (I - DT_s)\psi_{s,dq}(k) + T_s u_{s,dq}(k) - \frac{R_s T_s}{L_{sd}}\psi_{r,dq}, \tag{8}$$

$$i_{s,dq}(k+1) = E\left(\psi_{s,dq}(k+1) - \psi_{r,dq}(k+1)\right), \tag{9}$$

$$T_e(k+1) = \frac{3}{2}p_n\left(\psi_{s,dq}(k+1) \otimes i_{s,dq}(k+1)\right), \tag{10}$$

where I is the unit matrix, D is $\begin{bmatrix} R_s/L_{sd} & -\omega_r \\ \omega_r & R_s/L_{sq} \end{bmatrix}$, and $\psi_{s,dq}$ is the d-q axis stator voltage in the motor. $\psi_{r,dq}$ stands for $\begin{bmatrix} \psi_f & 0 \end{bmatrix}^T$, where $\begin{bmatrix} \psi_f & 0 \end{bmatrix}^T$ are the d-q axis stator and rotor magnetic chains, respectively, $u_{s,dq}$ is $\begin{bmatrix} u_{sd} & u_{sq} \end{bmatrix}^T$, where $\begin{bmatrix} u_{sd} & u_{sq} \end{bmatrix}^T$ are the d-q axis stator voltages of the motor, respectively, and T_s is a control cycle, where L_{sq} is equal to L_{sd} because the motor in this paper is a BLDCM, where $E = \begin{bmatrix} 1/L_{sd} & 0 \\ 0 & 1/L_{sd} \end{bmatrix}$, $i_{s,dq} = \begin{bmatrix} i_{sd} & i_{sq} \end{bmatrix}^T$, i_{sd}, and i_{sq} are the currents on the stator d-q axis in the motor.

The above three equations then predict the future states of the stator magnetic chain, current, and torque of the FCS-MPTC control system.

Conventional FCS-MPTC tends to select the stator electromagnetic torque and magnetic chain as evaluation conditions. The weight coefficients of the value function will have a moderating effect on the evaluation results and play a large part in the system's choice of the optimum value. However, in online prediction, errors as well as errors due to deviations can occur. So the focus of this paper's research is on how to deal with the impact of errors and biases online and how the weight coefficients should be adjusted.

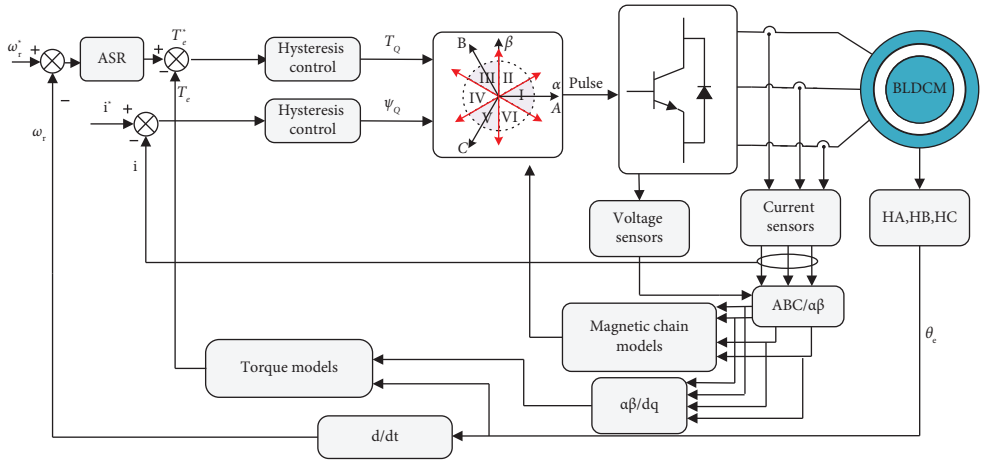

Figure 3: Basic schematic of the DTC.

The traditional value function is shown in the following equation. The schematic diagram of the traditional MPTC is shown in Figure 4.

$$g = \lambda_1 \left(T_e^* - T_e(k+1)\right)^2 + \lambda_2 \left(\psi_s^* - \psi_s(k+1)\right)^2, \quad (11)$$

where λ_1 and λ_2 are the weighting factors for regulating torque and stator chain errors, respectively.

4. Optimization Algorithm

4.1. WOA. WOA simulates the unique bubble foraging method of whales. According to the literature [23], the algorithm is divided into three stages: encirclement foraging, spiral updating, and searching for prey. The algorithm obtains relevant information by searching for solutions, keeps approaching the solution set through constant encirclement and a spiral approach, and eventually finds the final solution, i.e., the optimal solution. The two most important variables of the algorithm are the optimal solution and the range of approaches to the optimal set of solutions.

In the encircling feeding phase, whales need to be informed of the specific location of their prey through group communication and keep approaching it. In the algorithm, let the whale population size be N, the search space dimension be d and the i-th value whale position be denoted as $X_i = (x_i^1, x_i^2, \cdots, x_i^d)(i = 1, 2, \cdots, N)$. Simulating the predation phase, the mathematical model is as follows:

$$\begin{aligned} D &= \left|C \cdot X_p(t) - X(t)\right|, \\ X(t+1) &= X_p(t) - A * D, \end{aligned} \quad (12)$$

where t is the current number of iterations; $X(t)$ is the individual position vector; $X_p(t)$ is the prey position vector (the current optimal solution); and A and C are the coefficient vectors, respectively, and are related in the following way:

$$\begin{aligned} A &= 2a * r_1 - a, \\ C &= 2 * r_2, \end{aligned} \quad (13)$$

where r_1 and r_2 are random numbers of [0, 1], respectively; a is a control parameter that decreases linearly from 1 to 0 as the number of iterations increases, i.e.,

$$a(t) = 2 - \frac{2t}{\max_{\text{iter}}}, \quad (14)$$

where $\max_{\text{iter}}$ is the maximum number of iterations.

Once the location of the prey is known, the whale will often adopt a spiral approach in order to ensure a successful capture, mathematically modelled as follows:

$$X(t+1) = D * e^{bl} * \cos(2\pi l) + X_p(t), \quad (15)$$

where b is a constant used to bound the shape of the logarithmic spiral; l is a random number of [−1, 1].

The traditional WOA frequently introduces probabilities p to discriminate which location update is performed by an individual whale, p ranging from 0 to 1, and segments the mathematical model according to p, as shown in the following equation:

$$X(t+1) = \begin{cases} X_p(t) - A * D, & p < 0.5, \\ D * e^{bl} * \cos(2\pi l) + X_p(t), & p \geqslant 0.5. \end{cases} \quad (16)$$

The algorithm often requires a value to determine which stage it is at; here, it is necessary to determine whether it is the prey search stage or the encircling predation stage. Here, it is proposed that when $|A| > 1$, the whale is unable to obtain valid information about the prey, and then it needs to keep trying to search for cue information through random methods. Here, it is the equivalent of an insurance measure for unsuccessful predation. The mathematical model is as follows:

$$\begin{aligned} D &= \left|C \cdot X_{\text{rand}}(t) - X(t)\right|, \\ X(t+1) &= X_{\text{rand}}(t) - A * D, \end{aligned} \quad (17)$$

where $X_{\text{rand}}(t)$ is a randomly selected vector of individual positions from the current population. Figure 5 shows a three-dimensional plot of the baseline function for the WOA run.

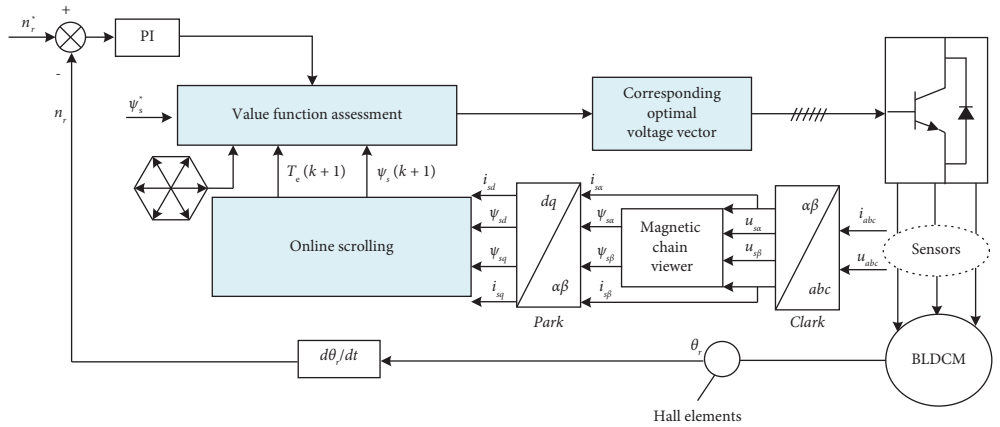

Figure 4: Schematic diagram of a conventional MPTC.

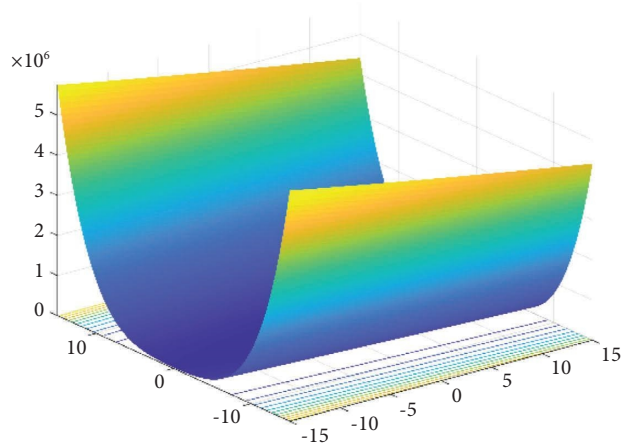

Figure 5: Three-dimensional view of the WOA operational benchmark function.

4.2. IWOA. For the population iteration of the population intelligence optimization algorithm, the good or bad quality of the initial population affects the search efficiency of the algorithm and the diversity of the population, both of which help a lot to improve the global convergence speed and the quality of the solution of the algorithm. In traditional WOA for solving optimization problems, there is no a priori knowledge system for the global optimal solution of the problem, which is unevenly distributed and poorly diversified in the solution space and cannot effectively extract the useful information from the solution space, which affects the search efficiency of the algorithm to some degree. The global and local search abilities of the WOA algorithm depend heavily on the value of the parameter A, which, according to (13), changes with the Convergence factor a; equivalently, the global and local search abilities of WOA depend on adjusting the convergence factor a. In the basic WOA, the convergence factor a decreases linearly to 0 with the number of evolutionary iterations from the set parameter, i.e., ideally the WOA can explore a larger and broader search area in the initial exploration because the initial value a is set very large, and as the algorithm advances, a gradually becomes smaller, which satisfies the local accurate search of the algorithm. However, WOA is nonlinearly changing in the evolutionary search process, and the linearly decreasing convergence factor a cannot fully reflect the actual optimization of the algorithm's search process, so this paper introduces a random convergence factor so that the convergence factor changes nonlinearly and dynamically with the increase in the number of iterations in order to balance the traditional global search and local search capabilities. The degree of deviation in (19) is the vector gradient of the convergence factor a. In this MPTC paper, the IWOA directly adjusts the weight coefficients of the objective function and outputs the optimal vector by equating the predicted value and the reference value of the objective function as the measured value and the estimated value, calculating the degree of deviation from its mathematical expectation, and iterating continuously.

WOA often takes a random initialization approach when dealing with initialized populations, which can lead to a high degree of randomness in the method, which is not conducive to reducing search time and does not guarantee population diversity. In this paper, we propose a backward learning improvement method to ensure population diversity and reduce computing time. The improvement method is to generate the reverse solution of the feasible solution, evaluate the reverse solution, and select a better candidate solution. In general, the opposite number is closer to the optimal solution than a random number. The mathematical model is as follows:

$$x_i^o = lb_i + ub_i - x_i, \tag{18}$$

where x_i is the individual feasible solution, x_i^o is its inverse solution, and lb_i and ub_i are the upper and lower bounds of the solution.

WOA is prone to local optimality as well as premature convergence during and after local development, and when perturbed, the algorithm can create the problem of difficulty in reaching an optimal solution. In this paper, we propose a random adjustment of the convergence factor strategy to simulate the perturbation operation on the population and produce more individuals to deal with the impact of sudden

deviations and errors. The mathematical model is shown in the following equation:

$$a(t) = a_{\text{initial}} - (a_{\text{initial}} - a_{\text{final}})\text{rand}() + \sigma r \text{and} n(), \quad (19)$$

where a_{initial} and a_{final} are the initial and termination values of the convergence factor, respectively. $r\text{and}()$ is used to simulate the perturbation, and σ is used to measure the deviation of the random variable from its mathematical expectation. The IWOA flowchart is shown in Figure 6. The pseudocode of IWOA is listed in Table 1.

5. MPTC with IWOA

The cost function of the conventional MPTC does not take into account the number of switches and is generally controlled by the relative error rate of the magnetic chain and the torque error rate, omitting the setting of the weighting factor, which does not correspond to the actual operating conditions, expressed as follows:

$$g = \sqrt{\left[\frac{T_e(k+1) - T_e^*(k)}{T_e^*(k)}\right]^2 + \left[\frac{\psi_s(k+1) - \psi_s^*(k)}{\psi_s^*(k)}\right]^2}, \quad (20)$$

$T_e^*(k)$ is the stator magnetic chain at moment k. $\psi_s^*(k)$ is the torque reference at moment k.

However, in actuality, the switching frequency of the inverter is not constant at low speeds, and the loss increases. MPTC applies the idea of optimization to solve the value function in real time, in order to get the ideal voltage vector for the inverter. In reality, however, the low-speed state will cause the inverter switching frequency to fluctuate and the loss to rise, which will also cause the controller settings to be challenging to modify and the dynamic performance to suffer. It is crucial to take the average switching frequency loss into account in order to avoid this circumstance. Similar to how the inverter increases the harmonic content of the output and decreases the overall efficiency of the entire drive system due to the numerous switching devices, the difficulty of the midpoint voltage balance, and the high cost of the system, the switching frequency constraints are added to the value function to achieve the presentation of the optimal control effect in the following work simulation.

Torque and flux performance, as well as average switching frequency minimum losses, are prioritized in this paper. The average switching frequency considers the period differently from the first two, so the number of switches is generally used instead of the average switching frequency, taking into account the following cost function for the number of switches.

$$g = \sqrt{\lambda_1\left[\frac{T_e(k+1) - T_e^*(k)}{T_e^*(k)}\right]^2 + \lambda_2\left[\frac{\psi_s(k+1) - \psi_s^*(k)}{\psi_s^*(k)}\right]^2 + \lambda_{sw} n_s}, \quad (21)$$

where λ_1, λ_2, and λ_{sw} represent the weighting factors of the three objective functions, respectively; n_s is the number of switching operations caused by the voltage vector applied at this point.

The cost function needs to be adjusted to achieve different control effects by setting different weighting factors to adjust the relative importance of each target. In this paper, the IWOA is used to adjust the parameters in due course to determine the weighting coefficients according to the variation of the magnetic chain, torque, and average switching frequency under different weights. In this paper, the relative importance of the target is seen by defining the square root error of torque pulsation, the square root error of chain pulsation, and the average switching frequency, and they are denoted in the following, respectively. Also, the evaluation function of the MPTC modified by IWOA is as follows:

$$\begin{aligned} T_{\text{RMSE}} &= \sqrt{\frac{\sum_{i=1}^{n}(T_e - T_e^*)^2}{n}}, \\ \psi_{\text{RMSE}} &= \sqrt{\frac{\sum_{i=1}^{n}(\psi_s - \psi_s^*)^2}{n}}, \\ f_{\text{avg}} &= \frac{N_s}{6t}, \\ m_{\text{avg}} &= \frac{\sum_{i=1}^{n}\sqrt{\lambda_1\left[T_e - T_e^*/T_e^*\right]^2 + \lambda_2\left[\psi_s - \psi_s^*/\psi_s^*\right]^2} + \lambda_{sw} n_s}{n}. \end{aligned} \quad (22)$$

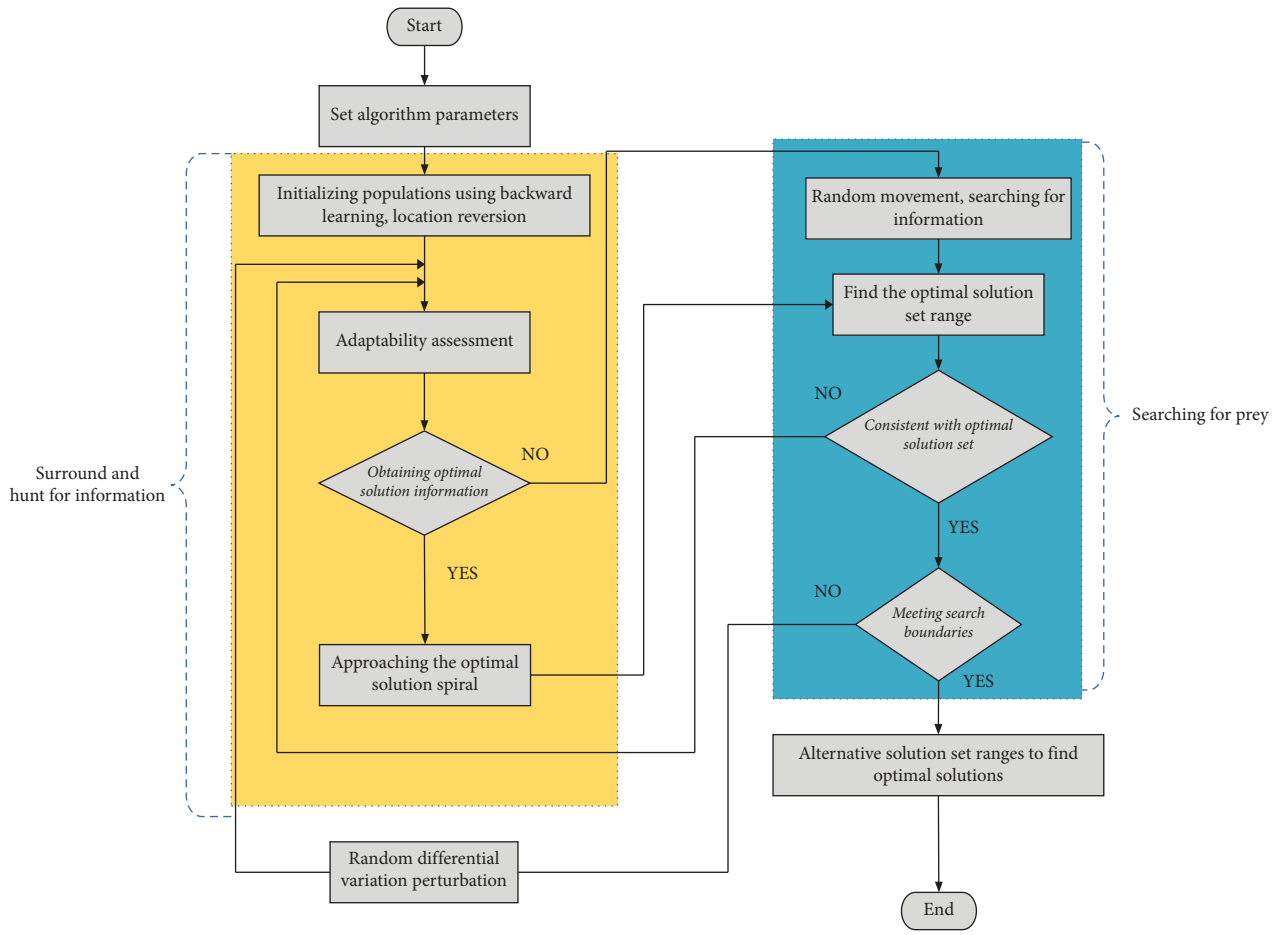

Figure 6: The IWOA flowchart.

Table 1: Pseudocode of IWOA.

(1) Setting the population size to produce an initialized whale population $\{X_i, i = 1, 2, \cdots, N\}$
(2) Calculate the fitness of each individual in the population $\{f(X_i), i = 1, 2, \cdots, N\}$; and record the current optimal individual and position;
(3) While $(t < t_{\max})$ do
(4) For $i = 1$ to N do
(5) Calculate the value of the convergence factor a
(6) Updating the values of other parameters
(7) If $(p < 0.5)$ do
If $(|\mathbf{A}| < 1)$ do
(8) Update the position of each individual;
(9) Else if $(|\mathbf{A}| \geqslant 1)$ do
(10) Randomly select an individual in the group
(11) Update the location of each individual
(12) End
(13) Else if $(p \geqslant 0.5)$ do
(14) Update the location of each individual
(15) End
(16) End
(17) For the optimal individual in the current population add a stochastic convergence factor strategy
(18) Calculating individual fitness in a population
(19) Update the current optimal individual and position
(20) $t = t + 1$
(21) End

WOA is essentially the reduction of the relative error between the training set and the prediction finger, while IWOA in this study employs a random adjustment of the convergence factor strategy to generate simulated perturbations and increase the number of predictions, taking into account a variety of situations to measure the degree of deviation from the target random variable by σ. The σ for the situations that exist for different target values is different.

λ_1 represents the weighting factor for torque, which is often the most important in a BLDCM, and because of the special structure of the BLDCM and the drive method, factor λ_1 is set at 5–25, and its σ_1 requirement is also the lowest, with σ_1 being the most important value to consider, set at 0.02–0.05 in this study. λ_2 is the weighting factor for flux and is usually limited to 2–10; σ_2 will be larger than σ_1 for torque and is usually set to 0.2–0.6. λ_{sw} is the average switching frequency weighting factor, an excessive increase will distort the current, usually set to 0.01–0.04 and 1.0–1.6 for σ_3. λ_{sw} is the least preferred value in the simulation, a conjecture that will be demonstrated in the next section.

Because the upper and lower limits are different for each target in the IWOA, the BLDCM requires an upper limit of 10 N.m. The upper limit for electromagnetic flux ripple is 0.05 V.s. The average switching frequency is set

between 2 and 7 kHz, depending on the actual inverter specification. The IWOA development parameters are shown in Table 2.

6. Results and Discussion

In order to test the effectiveness of the MPTC with the IWOA control algorithm in BLDCM, the simulation was carried out in MATLAB on a PC with 16 GB of memory and the simulation software MATLAB 2020b. The motor parameters in the simulation are listed in Table 3.

To highlight the superiority of IWOA, IWOA, WOA, DA, ACO, and GWO were simulated in the same environment using the same test functions as in the previous section, and their final fitness values were $1.63 * 10^5$, $1.78 * 10^5$, $3.58 * 10^5$, $2.08 * 10^5$, $2.26 * 10^5$, respectively.

Here, we can see from Figure 7 that IWOA converges the fastest. IWOA is roughly similar to WOA, so the convergence rate is similar. It is observed that the final fitness values of DA, ACO, GWO, and WOA are all larger than IWOA because the other algorithms tend to fall into local optima compared to IWOA, resulting in large fitness values. Figure 8 shows the iteration times of the five algorithms, which show the high efficiency of IWOA in processing functions.

In previous work, MPTC has often used a trial-and-error approach by gradually increasing the weights, identifying the optimum weighting factor based on the variation of different weights. This is unrealistic in practical engineering and can seriously affect the lifetime of the motor. In this study, IWOA is used to generate simulated perturbations using a unique random adjustment convergence factor strategy to measure the degree of deviation from the target by σ, which greatly reduces the time to run the motor to stability. Figure 9 shows the relationship between the three targets (root mean square error of torque pulsation, root mean square error of flux pulsation, and average switching frequency) and their weighting factors for the simulation 0–2 s, respectively.

Here, it can be observed that the root mean square error of torque pulsation and the root mean square error of flux pulsation both find their lowest values in the running time, verifying the high efficiency of IWOA as just described. In Figure 9(c), we find that the average switching frequency tends to decrease significantly as the weighting factor increases, and we cannot see the optimum value through the relationship. By confirming the optimum position of the weighting factor for torque and flux, the evaluation function is put together with the average switching frequency, and by applying a disturbance and changing the load torque to simulate light and heavy loads, it is observed whether the average switching frequency will have a large effect on the value function and how the weighting factor for the average switching frequency is taken.

As seen in both cases of Figures 10(a) and 10(b), the average switching frequency values are different for different loads, showing a decrease with increasing load. However, in both cases, the weighting factors of the average switching frequency coefficients corresponding to the inflection points of the evaluation function differ very little, so the average

Table 2: IWOA parameters.

Parameters	Significance	Values
Pop_size	Population size	500
Iter_max	Number of iterations	1000
dim	Dimensionality	3

Table 3: Motor parameters in the simulation.

Parameters	Symbol	Value	Unit
Pairs of poles	p	2	
Moment of inertia	J	0.0003	Nms^2
Stator resistance	R_s	1.5	Ω
Equivalent inductance of phase windings	$L_s - M$	0.21	mH
Speed	N	1000	Rpm
Stator current	I_s	10	A
DC volage	V_{DC}	330	V
Friction coefficient	B	0.001	Nms/rad
Back-EMF constant	—	0.015	V/rad/s

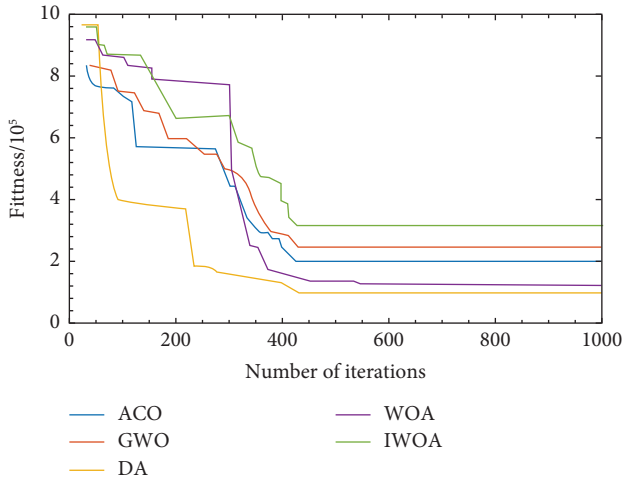

Figure 7: Final adaptation values for each algorithm.

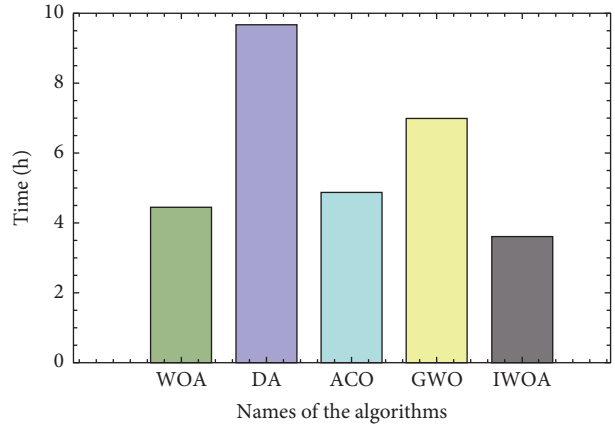

Figure 8: Iteration times for each algorithm.

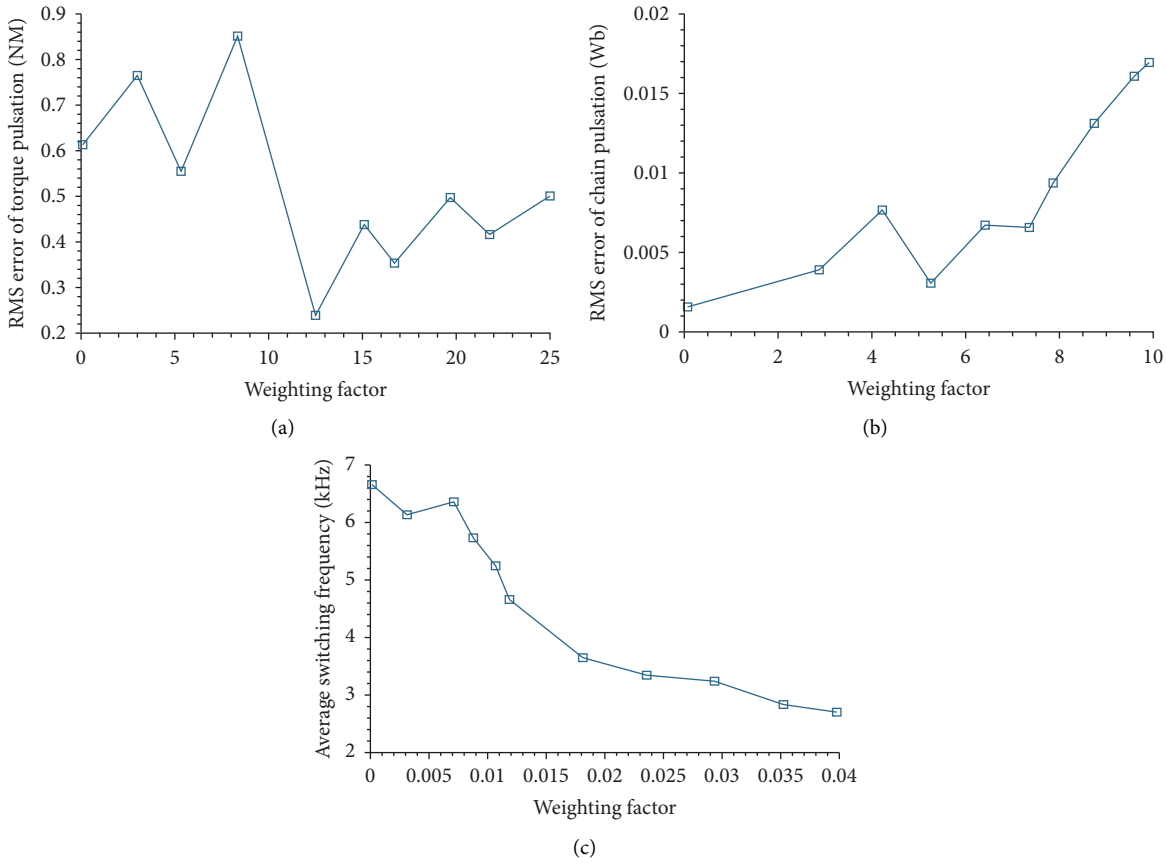

Figure 9: Target-weighting factor relationship. (a) Root mean square error of torque pulsation. (b) Root mean square error of flux pulsation. (c) Average switching frequency.

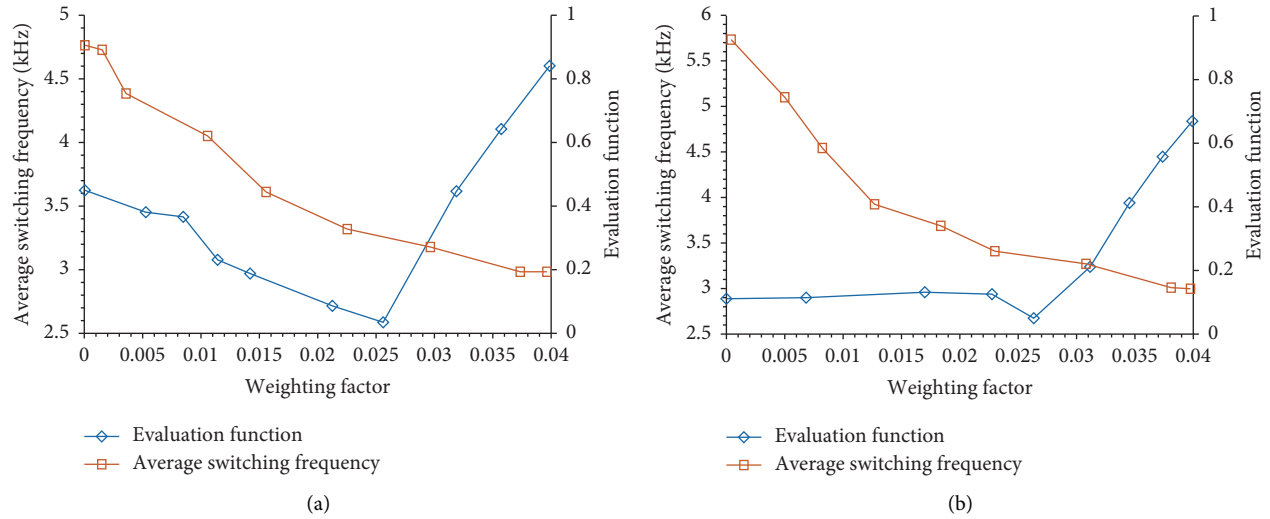

Figure 10: Average switching frequency and weighting factors corresponding to the value function. (a) Light load. (b) Heavy load.

switching frequency coefficients are set to [0.02, 0.03] in the following simulations.

The σ corresponding to the root mean square error of torque pulsation and the root mean square error of flux pulsation are shown in Figures 11(a) and 11(b), respectively. It can be seen that the deviation of both targets appears to be the lowest point in the same simulation time, and the deviation σ under the optimal weighting factor verified above is also the smallest, verifying the feasibility of the IWOA random adjustment of the convergence factor strategy.

The current, speed, electromagnetic torque, and counterelectromotive force of the BLDCM are studied and

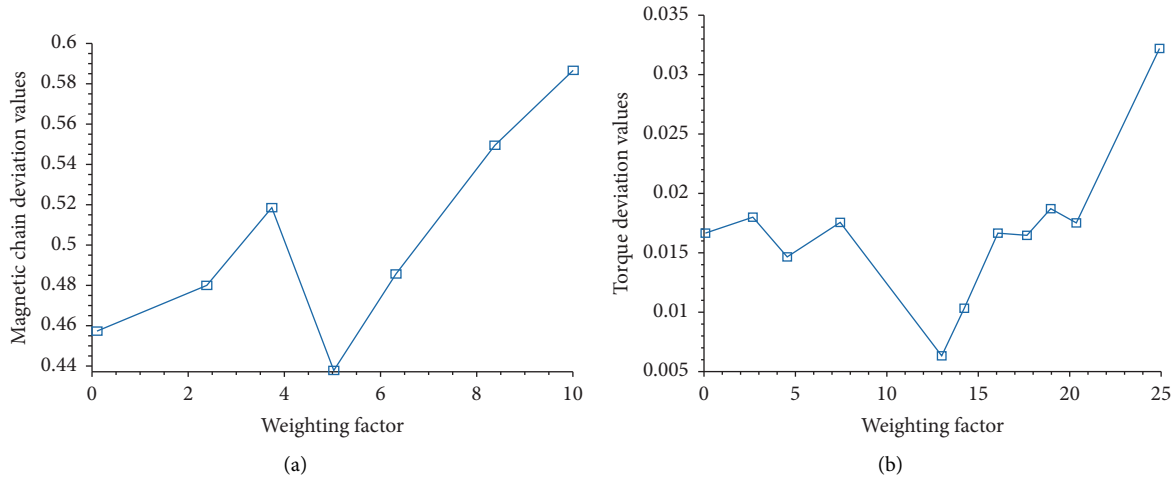

Figure 11: Weighting factors corresponding to target deviations. (a) Root mean square error of torque pulsation. (b) Root mean square error of flux pulsation.

simulated to compare the MPTC system under advanced algorithms. Since BLDCM is nowadays widely used in the scenario of electric vehicles, the proposed performance is studied under two conditions, the constant torque condition and the variable torque condition, to show the superiority of the algorithm by comparing the popular algorithms today. Figure 12 shows the flux capability of the proposed MPTC system under IWOA to control the BLDCM, and when the simulation reaches stability, the stator flux space vector trajectory controlled by the optimum switching frequency is plotted, and it can be clearly seen that IWOA has approximately 40% less high ripple than the original unadded MPTC system. As the BLDCM is a counterelectromotive force trapezoidal waveform, the stator flux trajectory position is dodecagonal.

Under constant torque conditions, the speed and torque performance, current waveforms, torque and speed errors, and rotor angular position are studied. Figures 13 and 14 show the reference speed and torque, respectively.

Figure 15 shows the current analysis of the BLDCM, which reaches a maximum of 28 A at 0.08 s and floats between −10 A and 10 A in the interval from 0.10 s to 0.4 s. A second maximum of 11A is reached in 0.4s and then floats steadily in the interval from −6 A to 6 A. Figure 16 shows the speed comparison analysis between the IWOA proposed in this paper and the advanced algorithm under the MPTC system. It can be seen that under the IWOA, the speed reaches the fastest 1006 rpm at 0.635 s and reaches stability at 0.64 s, while the WOA reaches the fastest 1008 rpm at 0.637 s, and at 0.647 s. The speeds in the MPTC system under these advanced algorithms oscillated to 995 rpm, 997 rpm, 998 rpm, and 1006 rpm, respectively, before gradually converging to the reference speed of 1000 rpm. Figure 17 shows the process from stabilization to stopping of the motor under each algorithm. It can be seen that IWOA stabilizes at 0 in 0.64 s, and the error control of the remaining algorithms is not very effective. Figure 18 shows the comparative analysis of each algorithm for torque. The torque reaches a peak of 53 N.m in the proposed IWOA at 0.08 s, drops to −40 N.m at 0.4 s, and then stabilizes at 6 N.m for the remainder of the time. The other algorithms are ineffective in dealing with the motor torque problem. Figure 19 shows a graph of the effectiveness of each algorithm in dealing with torque errors. From start to stable stop, IWOA controls the torque to 0 in only 0.4 s, verifying that IWOA has excellent performance in controlling torque with constant torque.

Table 4 shows a comparison of the error analysis of each technique in dealing with constant torque conditions for torque versus speed. The standard deviation reflects the degree of deviation of the results from the mean. A smaller standard deviation indicates a less discrete and more stable experimental result. It can be seen from the table that the standard deviation of torque and speed under IWOA is the lowest among the five algorithms, indicating that the experimental results are concentrated in a smaller range and the stability is the best compared to the other four algorithms. The mean value represents the convergence of the algorithms, and the IWOA mean value is also the smallest in both areas, indicating that the IWOA convergence accuracy is the most outstanding. Table 5 shows the motor performance of the MPTC system under the optimization of each algorithm to reach steady state. The cost analysis is based on the time required to reach motor steady state under the MPTC system without any algorithm as the standard value, and the superiority of IWOA can be seen from the performance indicators.

In the constant torque condition, the above demonstrates the superiority of the proposed IWOA. In response to the variable torque condition, the speed as well as the torque are observed and evaluated. In this case the speed remains the same as in the case above. Figure 20 shows the reference torque, which rises from a constant 6 N.m to 3 times 18 N.m in 1 s, and grayscales to 10 N.m in 1.5 s. Figure 21 shows the current waveform at IWOA, which reaches 43 A at 0.08 s, drops to −14 A at 0.42 s out, stabilizes in the −8 A–8 A interval from 0.4 s to 1.0 s, rapidly stabilizes to −18 A to 18 A at 1 s, drops from 18 A to 16 at 1.5 s, then stabilizes at −16 A to

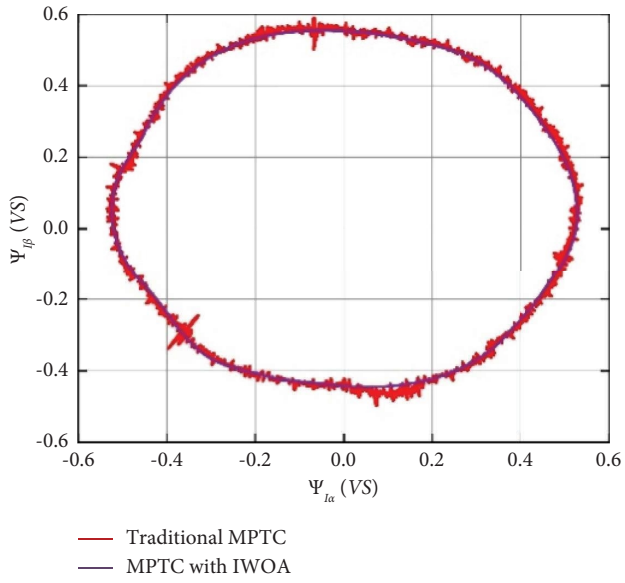

Figure 12: Comparison of the stator flux space vector trajectory under IWOA and conventional MPTC.

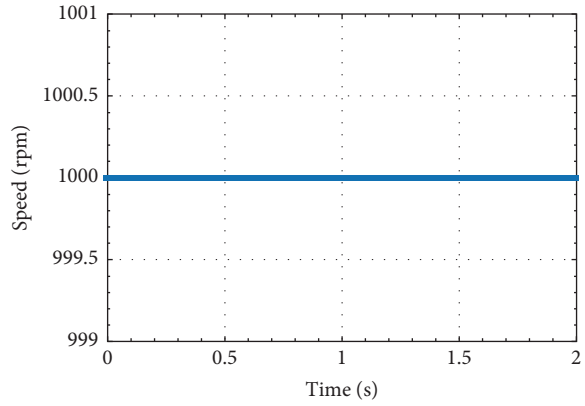

Figure 13: Reference speed at constant torque.

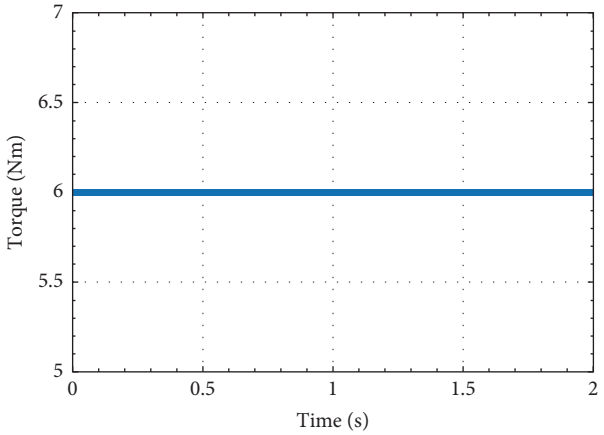

Figure 14: Reference torque at constant torque.

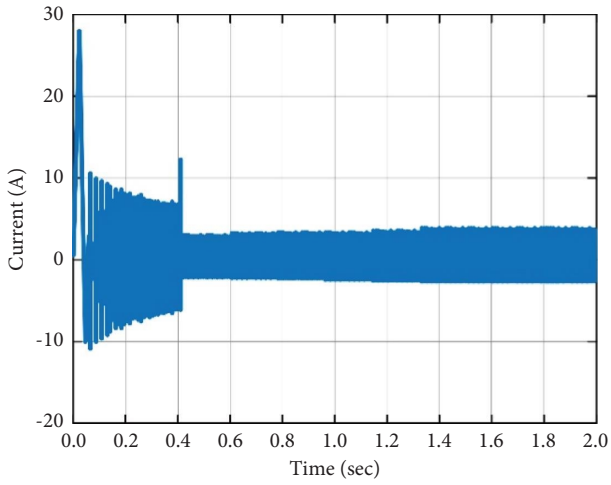

Figure 15: Current waveform at constant torque.

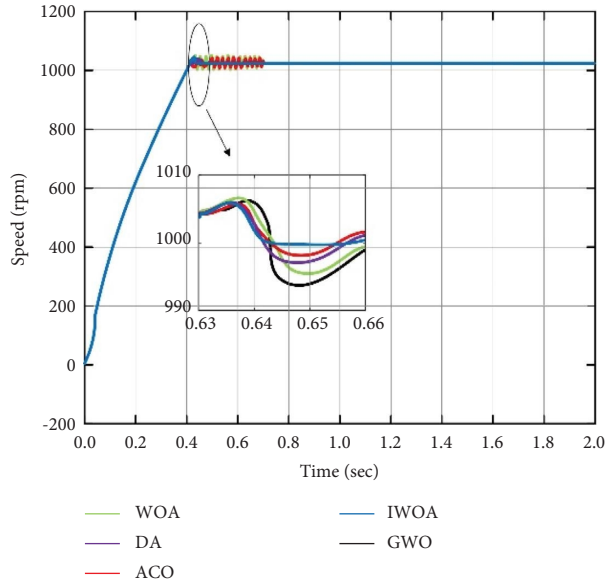

Figure 16: Speed comparison for each algorithm at constant torque.

16 A, verifying that the current increases as torque increases and decreases as it increases.

Figures 22 and 23 show the comparative speed analysis of each algorithm for the variable torque condition, respectively, obtaining the same results as for the constant torque condition. Figure 24 shows the comparative torque analysis. While the proposed algorithm reaches 10 N.m at 0.23 s, rises to 15 N.m at 1.00 s, drops to 9 N.m at 1.5 s, and gradually stabilizes, the rest of the algorithms are not very effective in dealing with variable torque, having a large amplitude phenomenon and strong jitter in the waveform. Table 6 shows the number of populations that reach the optimal solution for the solved model at five stages under the processing of variable torque problems. It can be observed that the IWOA shows a fast rising phase at 20%, 40%, and 60% stages with a continuous increasing number, and the

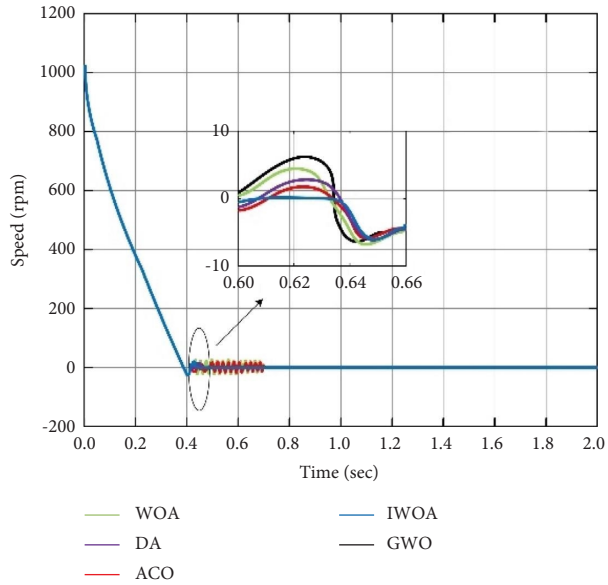

Figure 17: Comparison of errors in the speed of each algorithm at constant torque.

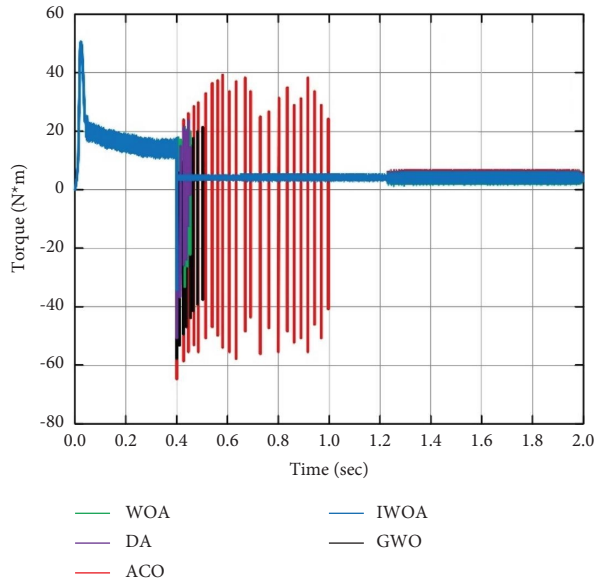

Figure 18: Comparison of the torque obtained by each algorithm at constant torque.

IWOA does not lose its equilibrium in stability due to torque changes, but enters another stable phase very smoothly. ACO, GWO, and DA in response to torque changes, lost their original accuracy and did not achieve the desired stability. WOA also had an increasing number of optimal solutions in the early period, but the results were not very impressive in the later period due to the low convergence accuracy. Table 7 shows a comparison of the efficiency of

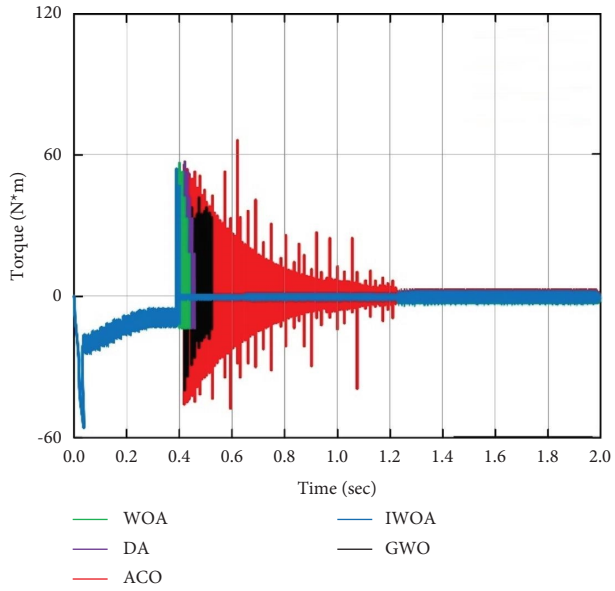

Figure 19: Comparison of torque errors for each algorithm at constant torque.

Table 4: Comparison of error analysis.

Solving techniques	Speed		Torque	
	Mean	Standard deviation	Mean	Standard deviation
WOA	$8.99E-108$	$2.55E-2$	0.00056	$5.55E-8$
DA	$7.56E-105$	$8.99E-5$	0.00189	$9.12E-9$
ACO	$6.88E-118$	$6.59E-4$	0.00285	$1.68E-12$
IWOA	$9.62E-180$	0	$5.62E-99$	$6.65E-16$
GWO	0.000056	2.62E-6	0.00089	$5.95E-8$

Table 5: Motor performance under optimization of each algorithm.

Solving techniques	Performance indicators			
	THD%	Torque ripple	Costs analysis	Power factor
WOA	8.66	18.34	0.952	0.952
DA	7.92	16.56	0.881	0.967
ACO	7.88	18.92	0.898	0.961
IWOA	4.33	6.62	0.627	0.992
GWO	7.26	15.89	0.914	0.975

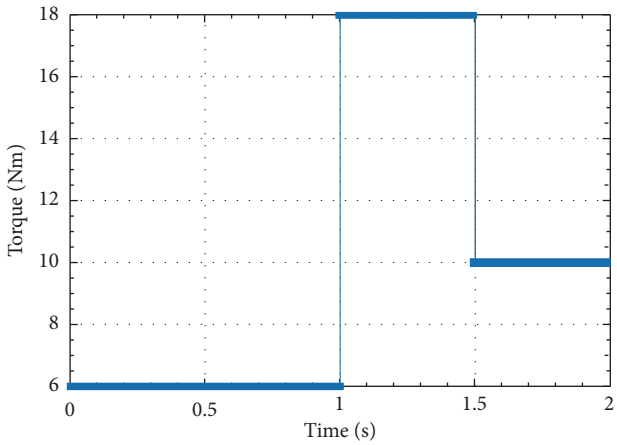

Figure 20: Reference torque at variable torque.

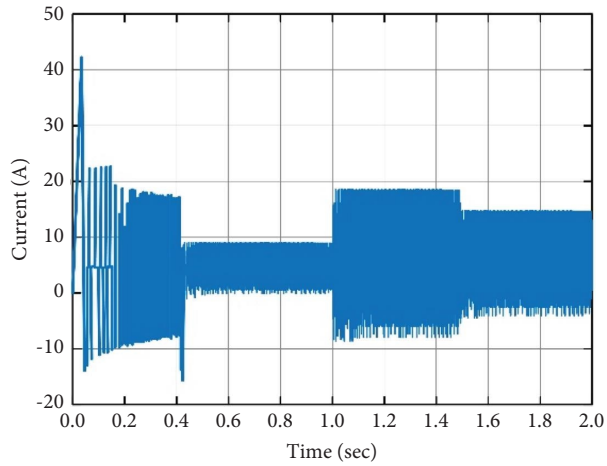

Figure 21: Current waveform at variable torque.

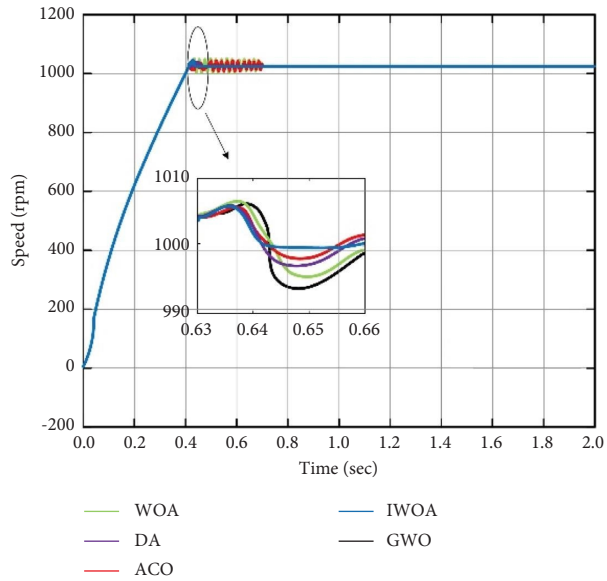

Figure 22: Speed comparison for each algorithm with variable torque.

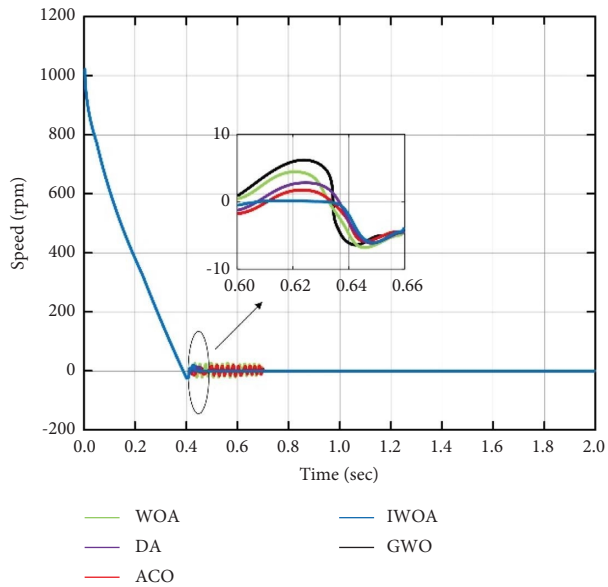

Figure 23: Comparison of speed errors for each algorithm under variable torque.

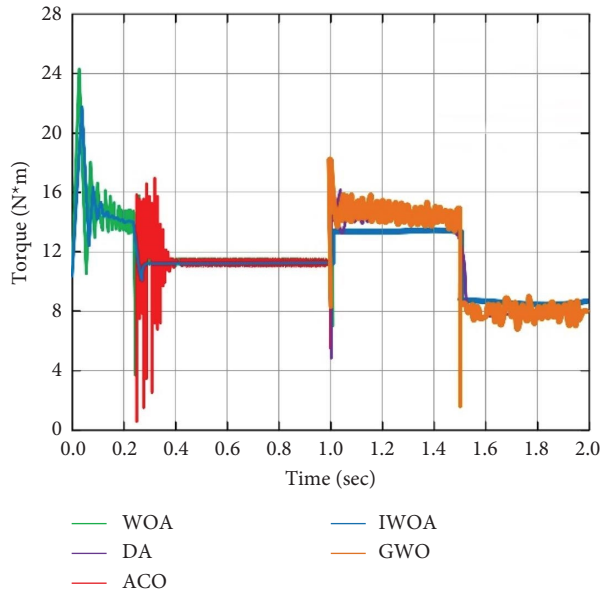

Figure 24: Comparison of the torque of each algorithm under variable torque.

Table 6: Population size of the optimal solution in the 5-stage model.

Range of population values (%)	Optimal solution values for advanced algorithms				
	WOA	DA	ACO	IWOA	GWO
20	26.5	29.5	28.4	30.4	36.5
40	29.8	36.8	30.6	42.5	39.4
60	30.8	30.5	27.2	56.5	28.6
80	25.1	29.5	21.5	58.9	19.7
100	24.9	25.8	28.7	58.2	29.5

Table 7: Comparison of the efficiency of each algorithm.

Solving techniques	Efficiency (%)
WOA	85.29
DA	87.31
ACO	87.92
IWOA	94.32
GWO	88.78

each algorithm applied to the MPTC system to deal with the problem. The above tables and figures can fully demonstrate the high efficiency of IWOA in solving the problems of speed error and torque pulsation, with better dynamic and steady-state performance and robust performance, to realize the coordinated and optimized control of electromagnetic torque and stator magnetic chain.

7. Conclusions

This paper presents an improved MPTC system based on IWOA for BLDCM control. The algorithm simulation data has better convergence, higher accuracy, and greater stability than WOA, DA, ACO, and GWO. The proposed method takes into account the BLDCM switching frequency losses, incorporates the idea of simulated disturbances, explores the corresponding weighting relationships of torque pulsation, magnetic chain pulsation, and switching frequency in the MPTC system, and finds a suitable interval for the target. In order to investigate the effectiveness of IWOA in MPTC systems, the simulations are compared with WOA, DA, ACO, and GWO in two different cases, and the simulation results show that the proposed method can better reduce torque pulsation and magnetic chain ripple with an efficiency of 94.32%. In future work, we will combine big data to make the proposed method even better and apply it to more complex industrial production.

Data Availability

The data used to support the findings of this study are available from the corresponding author upon request.

Conflicts of Interest

The authors declare that they have no conflicts of interest regarding the publication of this study.

Acknowledgments

The paper was supported by the Jilin Provincial Development and Reform Commission (Grant: 2022C045-11).

References

[1] W. Chen, Z. Liu, Y. Cao, X. Li, T. Shi, and C. Xia, "A position sensorless control strategy for the BLDCM based on a flux-linkage function," *IEEE Transactions on Industrial Electronics*, vol. 66, no. 4, pp. 2570–2579, 2019.

[2] S. Lee and S.-W. Baek, "A study on the improvement of the cam phase control performance of an electric continuous variable valve timing system using a cycloid reducer and BLDC motor," *Microsystem Technologies*, vol. 26, no. 1, pp. 59–70, 2020.

[3] X. Wang, X. Wu, S. Cheng, J. Shi, X. Ping, and W. Yue, "Design and experiment of control architecture and adaptive dual-loop controller for brake-by-wire system with an electric booster," *IEEE Transactions on Transportation Electrification*, vol. 6, no. 3, pp. 1236–1252, 2020.

[4] A. Joseph Godfrey and V. Sankaranarayanan, "A new electric braking system with energy regeneration for a BLDC motor driven electric vehicle," *Engineering Science and Technology, an International Journal*, vol. 21, no. 4, pp. 704–713, 2018.

[5] B. Tan, X. Wang, D. Zhao, K. Shen, J. Zhao, and X. Ding, "A lag angle compensation strategy of phase current for high-speed BLDC motors," *IEEE Access*, vol. 7, pp. 9566–9574, 2019.

[6] Y. Li, X. Song, X. Zhou, Z. Huang, and S. Zheng, "A sensorless commutation error correction method for high-speed BLDC motors based on phase current integration," *IEEE Transactions on Industrial Informatics*, vol. 16, no. 1, pp. 328–338, 2020.

[7] M. Aqil and J. Hur, "A direct redundancy approach to fault-tolerant control of BLDC motor with a damaged Hall-effect sensor," *IEEE Transactions on Power Electronics*, vol. 35, no. 2, pp. 1732–1741, 2020.

[8] X. Zhou, X. Chen, F. Zeng, and J. Tang, "Fast commutation instant shift correction method for sensorless coreless BLDC motor based on terminal voltage information," *IEEE Transactions on Power Electronics*, vol. 32, no. 12, pp. 9460–9472, 2017.

[9] X. Zhou, Y. Zhou, C. Peng, F. Zeng, and X. Song, "Sensorless BLDC motor commutation point detection and phase deviation correction method," *IEEE Transactions on Power Electronics*, vol. 34, no. 6, pp. 5880–5892, 2019.

[10] X. Zhou, X. Chen, C. Peng, and Y. Zhou, "High performance nonsalient sensorless BLDC motor control strategy from standstill to high speed," *IEEE Transactions on Industrial Informatics*, vol. 14, no. 10, pp. 4365–4375, 2018.

[11] H. Wu, H. Zhang, P. Cui, X. Zhao, and D. Zhang, "Compensation method of DC-link current integral deviation for sensorless control of three-phase BLDC motor," in *Proceedings of the 2022 11th International Conference on Communications, Circuits and Systems (icccas 2022)*, pp. 12–18, Singapore, May 2022.

[12] A. Usman and B. S. Rajpurohit, "Time-efficient fault diagnosis of a BLDC motor drive deployed in electric vehicle applications," in *Proceedings of the 2020 Ieee Global Humanitarian Technology Conference (GHTC)*, Seattle, WA, USA, October 2020.

[13] M. Wu, X. Sun, J. Zhu, G. Lei, and Y. Guo, "Improved model predictive torque control for PMSM drives based on duty cycle optimization," *IEEE Transactions on Magnetics*, vol. 57, no. 2, pp. 1–5, 2021.

[14] B. Kiani, S. Soleymani, B. Mozafari, and H. M. Shourkaei, "Model predictive based direct torque control for induction motor drives by sole-evaluation of two parameter independence duty ratios for each voltage vector," *Electric Power Components and Systems*, vol. 48, no. 19–20, pp. 2019–2036, 2021.

[15] Y. Yang, W. Song, and H. Ren, "Encoderless model predictive torque control of DTP-PMSM with sliding mode speed observer," in *Proceedings of the 6th Ieee International Conference on Predictive Control of Electrical Drives and Power Electronics (PRECEDE 2021)*, pp. 202–206, Jinan, China, November 2021.

[16] P. D. Kumar, T. Ramesh, and P. Ramakrishna, "Performance analysis of multi-level inverter-fed position sensorless PMSM drive using modified MPTC," *IETE Journal of Research*, vol. 43, no. 01, pp. 1–7, 2021.

[17] C. Gong, Y. Hu, M. Ma, J. Gao, and K. Shen, "Novel analytical weighting factor tuning strategy based on state normalization and variable sensitivity balance for PMSM FCS-MPTC," *IEEE*, vol. 25, no. 3, pp. 1690–1694, 2020.

[18] S. Mirjalili and A. Lewis, "The whale optimization algorithm," *Advances in Engineering Software*, vol. 95, pp. 51–67, 2016.

[19] H. Hu, T. Wang, H. Wang, and C. Wang, "Q-learning optimized diagonal recurrent neural network control strategy for brushless direct current motors," *Advances in Mechanical Engineering*, vol. 12, no. 9, Article ID 168781402095822, 2020.

[20] B. Naidu Kommula and V. Reddy Kota, "Design of MFA-PSO based fractional order PID controller for effective torque controlled BLDC motor," *Sustainable Energy Technologies and Assessments*, vol. 49, Article ID 101644, 2022.

[21] H. Yin, W. Yi, K. Wang, J. Guan, and J. Wu, "Research on brushless DC motor control system based on fuzzy parameter adaptive PI algorithm," *AIP Advances*, vol. 10, no. 10, Article ID 105208, 2020.

[22] H. Yin, W. Yi, J. Wu, K. Wang, and J. Guan, "Adaptive fuzzy neural network PID algorithm for BLDCM speed control system," *Mathematics*, vol. 10, no. 1, p. 118, 2021.

[23] J. H. Qin, W. R. Wang, and X. Yan, "Parameter tuning method for the controller of brushless DC motor based on Coyote algorithm," *Iranian Journal of Science and Technology, Transactions of Electrical Engineering*, vol. 46, no. 3, pp. 713–722, 2022.

[24] T. Wang, H. Wang, H. Hu, J. Qing, and C. Wang, "Lion swarm optimisation-based tuning method for generalised predictive fractional-order PI to control the speed of brushless direct current motor," *IET Electric Power Applications*, vol. 16, no. 8, pp. 879–895, 2022.

[25] Q. Zhang, J. Deng, and N. Fu, "Minimum copper loss direct torque control of brushless DC motor drive in electric and hybrid electric vehicles," *IEEE Access*, vol. 7, pp. 113264–113271, 2019.

[26] Y. Cao, T. Shi, X. Niu, X. Li, and C. Xia, "A smooth torque control strategy for brushless DC motor in braking operation," *IEEE Transactions on Energy Conversion*, vol. 33, no. 3, pp. 1443–1452, 2018.

[27] M. B. Shahid, W. Jin, M. A. Abbasi, A. R. Husain, and M. Hassan, "Torque error based auto-tuning of weighting factor in model predictive torque control of induction motor drive," *J. Electr. Eng. Technol.*, vol. 18, no. 3, pp. 1959–1973, 2023.

[28] K. Choi, Y. Kim, S.-K. Kim, and K.-S. Kim, "Computationally efficient model predictive torque control of permanent magnet synchronous machines using numerical techniques," *IEEE Transactions on Control Systems Technology*, vol. 30, no. 4, pp. 1774–1781, 2022.

[29] P. R. U. Guazzelli, W. C. de Andrade Pereira, C. M. R. de Oliveira, A. G. de Castro, and M. L. de Aguiar, "Weighting factors optimization of predictive torque control

of induction motor by multiobjective genetic algorithm," *IEEE Transactions on Power Electronics*, vol. 34, no. 7, pp. 6628–6638, 2019.

[30] A. Brodzicki, M. Piekarski, and J. Jaworek-Korjakowska, "The whale optimization algorithm approach for deep neural networks," *Sensors*, vol. 21, no. 23, p. 8003, 2021.

[31] X. Chen, "Research on new adaptive whale algorithm," *IEEE Access*, vol. 8, pp. 90165–90201, 2020.

[32] A. Got, A. Moussaoui, and D. Zouache, "A guided population archive whale optimization algorithm for solving multi-objective optimization problems," *Expert Systems with Applications*, vol. 141, Article ID 112972, 2020.

[33] S.-I. Han, "Fractional-order sliding mode constraint control for manipulator systems using grey wolf and whale optimization algorithms," *International Journal of Control, Automation and Systems*, vol. 19, no. 2, pp. 676–686, 2021.

[34] S. G. Malla, P. Malla, J. M. R. Malla et al., "Whale optimization algorithm for PV based water pumping system driven by BLDC motor using sliding mode controller," *IEEE Journal of Emerging and Selected Topics in Power Electronics*, vol. 10, no. 4, pp. 4832–4844, 2022.

[35] M. H. Nadimi-Shahraki, S. Taghian, S. Mirjalili et al., "EWOA-OPF: effective whale optimization algorithm to solve optimal power flow problem," *Electronics*, vol. 10, no. 23, p. 2975, 2021.